PRAMANA
— journal of
physics

Vol. 59, No. 1
July 2002
pp. 75–89

Effect of Nd^{3+} concentration on CW and pulsed performance of fiber-coupled diode laser pumped Nd:YVO_4 laser at 1064 nm

PRANAB K MUKHOPADHYAY, K RANGANATHAN, JOGY GEORGE,
S K SHARMA and T P S NATHAN
Diode Pumped Solid State Laser Group, Center for Advanced Technology, Indore 452 013, India
Email: pkm@cat.ernet.in

MS received 4 September 2001; revised 17 January 2002

Abstract. The effect of Nd^{3+} concentration on the CW and Q-switched laser performances at 1064 nm from Nd : YVO_4 has been studied under diode laser pumping in identical laser configuration. The Nd^{3+} concentrations used were 1, 2 and 3 at. % in YVO_4 crystals. Under the CW operations we have compared the thermal lensing effect, slope efficiencies and also the beam quality at the fourth-order degeneracy configuration. Q-switching was done with the help of an acousto-optic modulator and we have compared the pulses obtained from Nd : YVO_4 laser with different doping concentration. It was found that the 1 at.%-doped crystal is the best, offering highest optical-to-optical conversion efficiency (55%), lowest fractional heat load (24%), highest pulse energy (80 μJ) and shortest pulse width (20 ns). It was also found that there was not much difference in performances for 2 and 3 at. %-doped crystals both in CW and Q-switched configurations.

Keywords. Thermal lens; diode pumping; mode degeneracy; Q-switching; AO modulator; Nd : YVO_4 crystal.

PACS Nos 42.60.Lh; 42.60.Da; 42.60.By; 42.55.Rz

1. Introduction

Nd : YVO_4 crystal has been confirmed to be a very efficient laser crystal for diode pumping [1–3] due to its large absorption coefficient and broad absorption bandwidth at the diode wavelength, large stimulated emission cross-section (25×10^{-19} cm^2) and narrow emission bandwidth (0.96 nm) at 1064 nm, and good thermal conductivity (0.0523 W/K-cm) . Moreover the Nd^{3+} concentration in YVO_4 can be as high as 3 at.% in order to increase the absorption linewidth and peak absorption cross-section at the diode emission wavelength at 809 nm. But these advantages are generally offset by the fluorescence quenching effect in Nd : YVO_4 crystal [4]. Hence there should be an optimum Nd^{3+} concentration in YVO_4 in order to have high wall plug efficiency.

Earlier work on the effect of Nd^{3+} doping level was mainly concentrated on the laser efficiency and thermal fracture point of view in CW mode of operation [5,6]. Recently a re-

port on the effect of Nd^{3+} concentration on the strength of the thermal effects in $Nd:YVO_4$ laser has been described in [7]. However, our current work addresses several important issues related to the diode-pumped $Nd:YVO_4$ lasers which are not considered in [7]. In this paper we report our experimental observations on the effect of Nd^{3+} concentration on many important laser parameters involved with the CW operation as well as the acousto-optically Q-switched operation.

The paper is organized as follows: In §2, we describe the experimental set up in details. In §3 we report the thermal lensing effect in $Nd:YVO_4$ crystal with different Nd^{3+} concentration and calculated the fractional heat load from the experimental data. In §4 we report a characterization of the CW laser performance with varying doping level under diode laser pumping. In the same section we report the characterization of the output beam from the $Nd:YVO_4$ laser with different doping level at the fourth-order degeneracy configuration. In §5 we report the influence of doping concentration on the acousto-optically Q-switched laser performance of $Nd:YVO_4$ crystal. In this section we compared the pulse energy and pulse width as a function of the absorbed pump power and repetition rate for three different doping concentrations. In §6 we summarize the results obtained in the previous sections.

2. Experimental details

The $Nd:YVO_4$ crystals we have compared were obtained from Gospel Opto-electronic Technology, P.R. China. The performance comparison was done for three Nd^{3+} doping levels in YVO_4, namely 1, 2 and 3 at.%. All these crystals had a face area of 3 mm $\times$ 3 mm and lengths of the crystals were chosen in such a way that nearly the same amount of pump power was absorbed by the crystals. The thickness of the crystals were 1.5, 1.0 and 0.5 mm for 1, 2 and 3 at.%-doped crystals respectively.

Absorption measurements at the diode wavelength ($\sim$809 nm) were done by measuring the transmitted diode power through the crystal with respect to the incident pump power. 1 at.%-doped crystal absorbed 90% of the diode power with an effective absorption coefficient of 15.3 cm^{-1}, the 2 and 3 at.%-doped crystals absorbed 95% and 80% of the incident diode power with effective absorption coefficient 30 cm^{-1} and 32.2 cm^{-1} respectively.

All the crystals used in our experiments were *a*-axis cut. The stimulated emission cross-section for these crystals was 25×10^{-19} cm^2. $Nd:YVO_4$ shows fluorescence quenching effect for doping level more than 1 at.%. The fluorescence lifetime (τ_F) for 1 at.%-doped crystal was 98 μs and that for 2 and 3 at.%-doped crystals were 74 μs and 57 μs respectively [4].

The pumping scheme was identical for all the experiments. The pump source used was a fiber-coupled diode laser (Coherent F-81-1000C-SM-M) that delivered a maximum output power of 1 W. The wavelength of maximum emission at 25°C for this was 809 nm with a 1.2 nm spectral width (FWHM). The fiber tip had a diameter of 100 μm and a numerical aperture of 0.1. The spatial intensity profile of the output beam from the fiber was circular in shape with a maximum at the center and a far field divergence (FWHM) of 7.34° in the horizontal and 6.66° in the vertical directions respectively.

The output beam was collimated and focused using two plano-convex lenses (f = 25 mm) with a magnification of unity. Since the quality of the pump beam (M^2 parameter) and the actual focused spot size are two important parameters for overlap optimization of the pump and cavity modes [8], we have measured these two parameters for this set up. For

this purpose spot sizes at several locations after the focusing lens and around the focused position were estimated with the help of a knife-edge with 10% clip level criterion. Variation of the diode beam spot size was plotted with distance from the secondary principal plane of the lens and the focused spot radius and the M^2 parameter were estimated by least square fitting of the usual multimode beam propagation law given by

$$\omega_{\mathrm{p}}^2(z) = \omega_{\mathrm{p0}}^2 \left\{ 1 + \left[\frac{\lambda_{\mathrm{p}} M_{\mathrm{p}}^2}{n\pi\omega_{\mathrm{p0}}^2} (z - z_0) \right]^2 \right\}, \tag{1}$$

where ω_{p0} is the radius at the waist, λ_{p} the pump wavelength, M_{p}^2 the pump beam quality factor and z_0 the waist location from the focusing lens. The beam quality parameter and the focused spot radius estimated in this way were 16 and 62.5 μm respectively at the maximum operating current. Also, the average spot size within the crystals considering its absorption at the diode wavelength varies within 4% of the focused spot size and hence the average spot size can be considered to be the same as the focused spot size.

The laser diode junction temperature was kept at the value corresponding to optimum pump radiation absorption inside the crystal. It must be kept in mind that in OEM packaged laser diodes there is some thermal resistance between the diode junction and the temperature sensor; and with increasing thermal loads, the temperature difference of the two increases as well. In order to avoid the shift of laser wavelength with the current, diode output power was varied using neutral density filters, while keeping the diode operating current at its maximum value.

For all the laser experiments, we used a simple two-mirror resonator in semi-monolithic configuration. That is, the input mirror was directly deposited on one surface of the laser crystal and the other surface had anti-reflection coating at the lasing wavelength. The input mirror had a reflectivity more than 99.8% at 1064 nm and more than 95% transmission at the pump wavelength at 809 nm.

To measure the thermal lensing effect the resonator was made plane–plane type of 4.3 mm effective cavity length with 5% coupling. The pump power induces a lensing effect inside the gain medium and the plane–plane cavity reduces to a conventional plano-concave type resonator with the waist formed at the flat output coupler mirror. The waist radius and hence the thermal lens focal length was determined from the far-field divergence angle of the output beam. In order to measure the divergence of the output beam, the laser spot size was measured at a distance of 30 cm from the output coupler with the help of a knife edge with 10% clip level criterion.

For the CW laser experiments, we used a 7 mm long plano-concave resonator. The concave output mirror had a 80 mm radius of curvature with which the mode area at the gain medium became 87 μm ensuring good overlap between the pump and the cavity mode. We measured the slope efficiencies for the three crystals with output coupler reflectivity of 98.5, 95, 93, 91, 87 and 85% in order to compare their performances. The output beam was passed through a 808 cut-off filter in order to block the residual pump power and the power was measured with a power meter (Laser Precision Corporation).

To study the influence of Nd concentration on the beam waist shrinkage effect [9], we have chosen the fourth-order degeneracy configuration by keeping the cavity length around 40 mm. With this configuration, cavity mode size at the gain medium became 116 μm which was much larger than the pump spot size as required to observe the said effect.

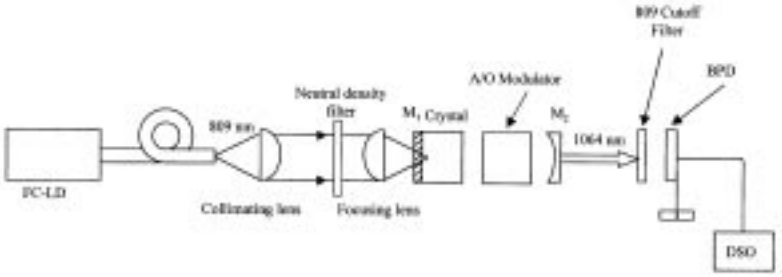

Figure 1. Schematic of Q-switching set up for $Nd:YVO_4$ laser using acousto-optic modulator.

The output coupler used for Q-switching experiments (figure 1) had a reflectivity of 95% with 200 mm radius of curvature. The geometrical cavity length in this case was 158 mm in order to accommodate the acousto-optic modulator. With intracavity AO Q-switch of 40 mm length (l_{AO}) and gain medium of 0.5–1.5 mm thickness (l_C), the equivalent free space of the cavity became

$$L_{\text{eff}} = L_{\text{geo}} - \left(l_{\text{AO}} - \frac{l_{\text{AO}}}{n_{\text{AO}}}\right) - \left(l_{\text{C}} - \frac{l_{\text{C}}}{n_{\text{C}}}\right) \tag{2}$$

where refractive index for Q-switch material was 1.46 and that of the laser crystal was 2.1. Thus the effective length of the resonator was 145 mm and the cavity mode radius at M_1 and M_2 were 174 μm and 332 μm respectively, with the waist formed at the plane mirror.

The Q-switcher (Gooch and Housego) used in our experiment had antireflection coating at 1.06 μm on both the faces and was driven at a 24 MHz center frequency with 22 W of rf power. The Q-switch was operated in the Bragg diffraction regime where the diffracted power was coupled to the first order only at an angle 6.7 mrad. The acoustic wave coupled to the Q-switch by the rf driver was shear type and hence the interaction was independent of the polarization of the laser beam. With an acoustic power of 22 W the single pass loss was 17% which was enough to cease the laser oscillation inside the cavity. In the case of acousto-optic Q-switching it is required that the switching time should be shorter than the pulse build up time in order to avoid multiple pulsing effect. The switching time can be estimated from the time taken by the acoustic wave to cross the mode diameter at the Q-switch, when the rf power is switched off. With a mode radius of 174 μm at the Q-switch and the velocity of shear wave inside the Q-switch material as 5.5 mm/μs, the switching time was estimated as 63 ns. The Q-switched output pulses were passed through an edge filter (RG850) to block the residual pump beam and were detected with the help of a biplanar photodiode. Average power was measured with the help of a power meter.

3. Thermal lens measurements

There are several mechanisms through which the absorbed pump power deposits heat into the solid state gain medium. One primary mechanism is the quantum defect which arises due to the difference in the pump photon energy and laser photon energy. Besides it, cross

relaxation and upconversion processes also lead to heat deposition into the gain medium. The non-uniform spatial intensity distribution of the diode laser beam profile leads to inhomogeneous steady state temperature distributions in the solid, which in turn leads to stresses, strains and displacements in the solid causing inhomogeneous change of refractive index of the crystal. For light propagating through the crystal, this inhomogeneous refractive index profile results in a variation of the phase front. The phase profile induced by the pumping beam creates a positive lensing effect due to the positive thermal-optic coefficient of the $Nd:YVO_4$ crystal.

For Nd^{3+}-doped YVO_4 crystal the contribution of the absorbed pump power towards the thermal lens formation due to the quantum defect does not depend upon doping concentration because the lasing wavelength does not change with the doping level. It is the cross relaxation process that depends on the doping concentration and can change the fractional heat load factor for the crystal and hence thermal lens focal length can vary with the doping concentration under identical pumping condition.

Focal length, f_{th}, of the pump power induced thermal lens for a fiber-coupled diode laser pumped $Nd:YVO_4$ crystal is given by [10]

$$\frac{1}{f_{\text{th}}} = \xi P_{\text{abs}} \frac{\left((\mathrm{d}n/\mathrm{d}T) + n\alpha_{\text{T}}\right)}{4\pi K_{\text{c}}} \frac{1}{w_{\text{pa}}^2} \tag{3}$$

where K_{c} is the thermal conductivity, P_{abs} the absorbed pump power, n the refractive index along the c-axis of the $Nd:YVO_4$ crystal, $\mathrm{d}n/\mathrm{d}T$ the thermal-optic coefficient of n, α_{T} is the thermal expansion coefficient along the a-axis and w_{pa} the pump spot size averaged over the length of the crystal.

Besides the thermal effect, mechanical stress can also cause variation of the phase profile across the medium, although the mechanical stress due to absorbed pump power is taken care by the thermal lens itself. The mechanical stress due to other factors like mounting of crystals can give rise to the change in refractive index profile across the medium [11]. If f_{m} is the focal length of the lens generated in the crystal due to these mechanical factors, then the effective focal length f_{e} will be given as

$$\frac{1}{f_{\text{e}}} = \frac{1}{f_{\text{th}}} + \frac{1}{f_{\text{m}}} = (\xi \alpha P_{\text{abs}} + \beta) \tag{4}$$

where α and β are two constants whose value do not depend on the doping concentration, and are given by

$$\alpha = \frac{\left((\mathrm{d}n/\mathrm{d}T) + n\alpha_{\text{T}}\right)}{4\pi K_{\text{c}}} \frac{1}{w_{\text{pa}}^2}, \tag{5}$$

and

$$\beta = \frac{1}{f_{\text{m}}}. \tag{6}$$

The value of α for an a-cut $Nd:YVO_4$ crystal and with the present pumping scheme is calculated for the following parameters: $K_{\text{c}} = 0.0523$ W/K-cm, $n = 2.165$, $\mathrm{d}n/\mathrm{d}T = 3.0 \times 10^{-6}$/K, $\alpha_{\text{T}} = 4.43 \times 10^{-6}$/K and $w_{\text{pa}} \approx 62.5 \times 10^{-4}$ cm. With these parameters the

value of α was found to be 0.0005 mW^{-1} cm^{-1}. Thus ξ and β remained to be two unknown parameters which were found by least square fitting to the experimentally measured thermal lens focal length values.

Thermal lens focal length and its variation with the pump power was experimentally measured by measuring the waist size formed at the output coupler mirror. The beam waist for a plane–plane cavity stabilized by thermal lens is given by

$$w_0^2 = \frac{\lambda L}{\pi}\sqrt{\frac{f_\mathrm{e}}{L} - 1} \tag{7}$$

where w_0 is the beam waist radius, L the effective cavity length, f_e the effective focal length and λ the laser wavelength. The beam waist was measured by measuring the far field divergence angle and by applying the Gaussian beam propagation law. It is to be noted that eq. (7) is valid for the TEM_{00} mode and hence corrections must be made for the higher order modes. In our experiments we have verified that the output beam was fundamental Gaussian with $M^2 = 1$.

Points in figure 2 show the thermal lens focal length and its variation with pump power for 1, 2 and 3 at.%-doped $\mathrm{Nd:YVO_4}$ crystals for identical pump and cavity configurations. The measurement errors in the thermal focal length was estimated from the maximum possible measurement errors in the far field spot size, effective cavity length and the knife edge position from the beam waist. The estimated error in the thermal focal length measurement was around 8%.

Solid lines in figure 2 are the least square fitting of the function given in eq. (4) with P_abs as the independent variable and with a value of α as 0.0005 mW^{-1} cm^{-1}, to the experimentally measured data points. The value of the fractional heat load was found

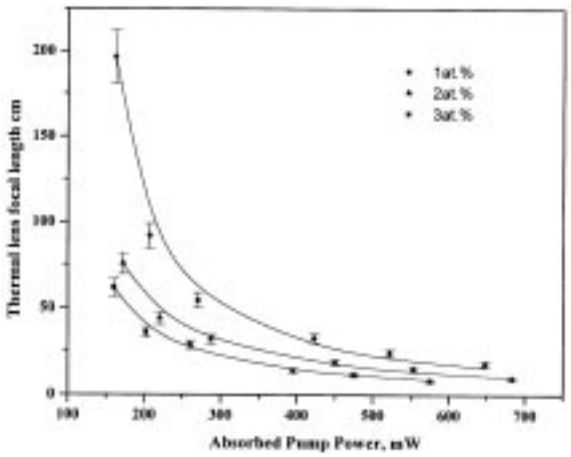

Figure 2. Variation of thermal lens focal length with the absorbed pump power for 1, 2 and 3 at.%-doped $\mathrm{Nd:YVO_4}$ crystal. The thickness of the crystals were 1.5, 1.0 and 0.5 mm respectively. Solid lines are the theoretical fitting of the function described in eq. (4). The value of the fractional heat load estimated from the fitting was 23.8, 32.8 and 45.5% for 1, 2 and 3 at.% doping. The focal power due to mounting was estimated to be -0.014, -0.015 and -0.02 cm^{-1} respectively.

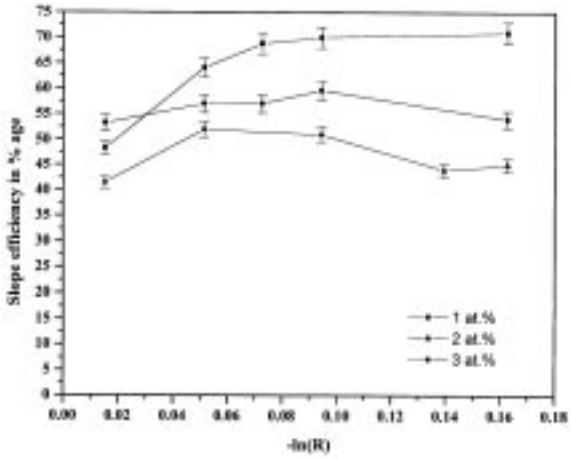

Figure 3. Variation of the slope efficiency with the output coupling for 1, 2 and 3 at.%-doped $Nd:YVO_4$ crystals. The slope efficiencies were measured with respect to the absorbed pump power.

to be 0.238 ± 0.01 for 1 at.%, 0.328 ± 0.02 for 2 at.% and 0.455 ± 0.04 for 3 at.%-doped crystals. It is worth mentioning here that the existing methods for determining fractional heat load for $Nd:YVO_4$ crystals are much more complicated in nature and used mainly 1 at.%-doped crystals [12,13]. It is to be noted that for 1 at.%-doped crystal the fractional heat load is exactly equal to the quantum defect value whereas 2 and 3 at.%-doped crystals show larger fractional heat load due to non-radiative cross-relaxation processes resulting from higher doping concentration. It is also to be noted that the focal power due to mechanical mounting is negative in sign and scales down with the thickness of the crystal as expected [11].

4. CW performances

We first measured the slope efficiencies for each crystal with different output coupler reflectivities ranging from 87–98.5%, all with 80 mm radius of curvature and under identical pumping configuration. In figure 3 we display the variation of the slope efficiencies with the output coupling. The output coupling values were determined as the negative of the logarithm of the mirror reflectivity. From figure 3 it can be found that for 1 at.%-doped crystal slope efficiency varies with output coupling similar to that expected for a homogeneously broadened crystal [14]. For homogeneously broadened crystal the slope efficiency is given by

$$\eta_s = \frac{T}{T+L}\frac{\lambda_p}{\lambda_l}\eta_c \tag{8}$$

where T is the output coupling, L the internal losses inside the cavity, λ_p and λ_l the pump and laser wavelengths and η_c the coupling efficiency of the pump beam and the cavity mode. η_c is a function of the pump spot size, cavity mode size and the saturation intensity

for the crystal. Since $Nd:YVO_4$ is a homogeneously broadened crystal, we expect from eq. (8) that the slope efficiency for $Nd:YVO_4$ should increase with the output coupling and saturate to a maximum value depending on the internal losses and the overlap efficiency. For 1 at.%-doped crystal we find that the maximum slope efficiency obtained for $Nd:YVO_4$ was 71% at an output coupling of 16% which is close to the theoretically possible slope efficiency, i.e., 76% whereas for 2 and 3 at.%-doped crystals we found a slight decrease in slope efficiency at higher output coupling contrary to eq. (8). Since the overlap efficiency does not change with the output coupling, the contribution of η_c towards the observed decrease of η_s at higher output coupling for 2 and 3 at.%-doped $Nd:YVO_4$ is ruled out. Such behavior can be explained as follows: The $\sigma\ \tau_F$ product for 2 and 3 at.%-doped crystal is much lower than that for 1 at.%-doped $Nd:YVO_4$ crystal due to the fluorescence quenching effect and hence they show higher threshold compared to that for 1 at.%-doped crystal under identical pumping and cavity configuration. Thus at higher output coupling the threshold population inversion becomes large enough for significant upconversion process rates [15] for these crystals. Due to this effect a significant fraction of the absorbed pump power is lost as heat and resulted in lower slope efficiencies for 2 and 3 at.%-doped crystals at higher output coupling.

In figure 4 we have plotted the inverse slope efficiency η_s vs. the inverse output coupling T, in order to find cavity losses for 1, 2 and 3 at.%-doped $Nd:YVO_4$ crystals. These parameters are related by [16]

$$\frac{1}{\eta_s} = \frac{1}{\eta_0} + \frac{L}{T\eta_0} \tag{9}$$

where η_0 is the intrinsic slope efficiency (for zero cavity losses). The inverse intercept yields $\eta_0 = 76\%$ for 1 at.%-doped crystal. For 2 and 3 at.%-doped crystals the intrinsic

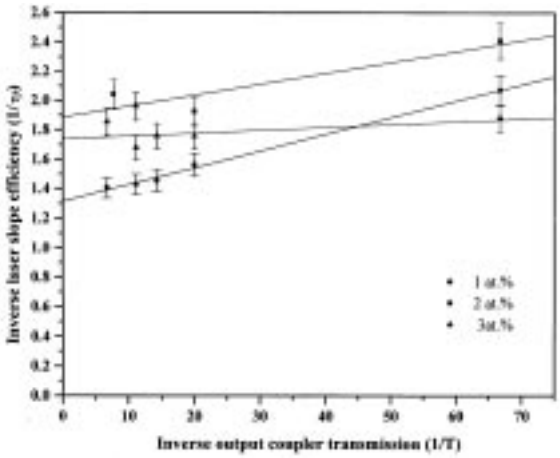

Figure 4. Inverse slope efficiency of diode pumped $Nd:YVO_4$ laser with different doping concentrations vs. inverse output coupler transmission. The Y-intercept and slope provide a measure of the intrinsic laser slope efficiency and the cavity losses respectively.

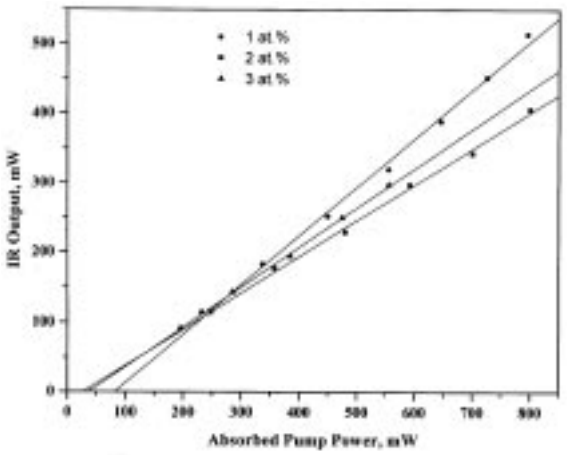

Figure 5. Slope efficiency curves for $Nd:YVO_4$ laser with different doping concentration at the optimum coupling. The optimum output coupling for 1 at.%-doped crystal was 9% whereas that for 2 and 3 at.%-doped crystals was 5%.

slope efficiency was found to be 53 and 57% respectively. It is to be noted that for 1 at.%-doped crystal the intrinsic slope efficiency is equal to the ideal value (= 809 nm/1064 nm) defined by the quantum defect. Moreover, by thermal lens experiments also we found that for 1 at.%-doped crystal the fractional heat load (ξ) was around 24%. This gives a full account for the absorbed pump power. Similarly for 3 at.%-doped crystal the total absorbed pump power can be accounted by measuring η_0 (57%) and ξ (45%). But for 2 at.%-doped crystal the value of η_0 and ξ were 53% and 33% respectively. There is a discrepancy of 14% of the absorbed pump power that we are unable to account for. Perhaps this is due to the non-uniform reflectivity of the mirror deposited on the crystal face. The slope times the η_0 indicates that the single pass cavity losses were 0.28%/mm, 0.2%/mm and 0.11%/mm for 1, 2 and 3 at.%-doped $Nd:YVO_4$ crystals respectively.

In figure 5 we report the input–output characteristics for the three crystals at the optimum output coupling. The optimum value of the output coupler reflectivity was found to be 91% for 1 at.%-doped crystal and 95% for 2 and 3 at.%-doped crystal. The optical-to-optical conversion efficiencies obtained were 55, 49 and 41% respectively. Though the slope efficiency obtained for 2 at.%-doped crystal was lower than that of 3 at.%-doped crystal it had shown higher optical-to-optical conversion efficiency due to its larger absorption at the pump wavelength.

We also have characterized the output beam for $Nd:YVO_4$ laser with varying doping concentration near the fourth-order mode degeneracy configuration. The order of degeneracy configuration is decided by the g_1 and g_2 values of the cavity ($g_i = 1 - L/R_i$, where L is the cavity length and R_i the radius of curvature). The configuration which satisfies $g_1 \times g_2 = 1/2$ is denoted as the fourth-order degeneracy because at this configuration the ratio of the longitudinal mode spacing to that of the transverse modes becomes equal to 4. It has been shown by Wu *et al* [9] that for a laser configuration where the cavity mode size is larger than the pump spot size, the fundamental mode shrinks in size at any mode degeneracy point allowing higher order modes to oscillate. This effect resulted in a drop in

output power and degradation of the output beam quality. We have chosen the fourth-order degeneracy point because at this configuration the ratio of the mode waist to pump spot size becomes maximum. In our semi-monolithic set up with 80 mm ROC of the coupler mirror this occurs at an effective cavity length of 40 mm, but with the thermal lensing effect this degeneracy point shifts towards the shorter cavity length. One way to find out the degeneracy location is to observe the drop in the output power [9]. In figure 6 we show how the output power varies with the cavity length near the fourth-order degeneracy point. We also characterized the beam quality at and away from the degeneracy point for 1 at.%-doped crystal. It can be found from figure 7 that the beam propagation factor (M^2 parameter) remains nearly at unity at all pump power levels at a cavity length which is away from the degeneracy location whereas at the degeneracy location the M^2 parameter increases with the absorbed pump power due to the oscillation of the higher order modes. This observation confirms that the fundamental mode is shrunk in size at the cavity length where mode degeneracy occurs. In figure 8 we show the variation of the output beam divergence with the cavity length near the fourth-order mode degeneracy location for 1, 2 and 3 at.%-doped crystals at the same amount of the absorbed pump power. The maximum divergence occurs at different locations for these crystals because the fractional heat load is different for these crystals. From figure 8 it is clear that the maximum mode shrinkage occurs for 2 at.%-doped crystal showing largest divergence, whereas for 1 and 3 at.%-doped crystal this effect is nearly the same. Also the region of nearly degenerate condition differs with doping. For 1 at.%-doped crystal this region is narrower compared to that for 2 and 3 at.%-doped crystal.

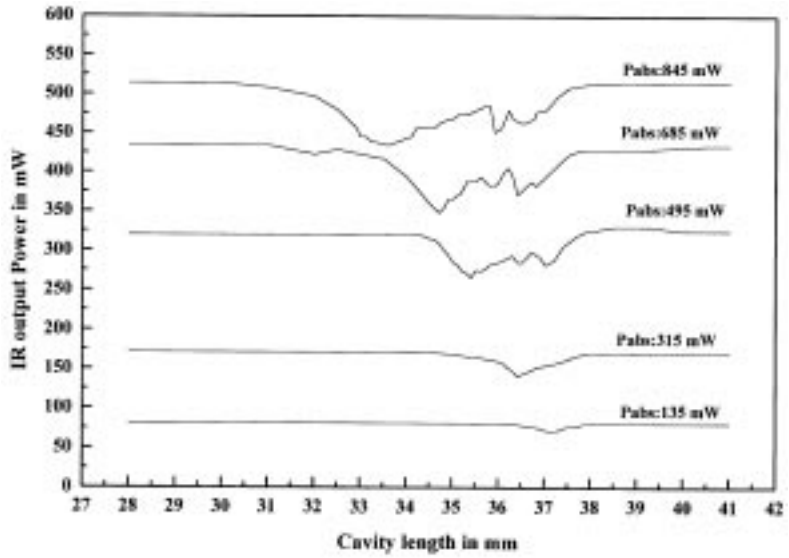

Figure 6. Output power from 1 at.%-doped $Nd:YVO_4$ laser as a function of the cavity length near the fourth-order degeneracy configuration at different absorbed pump power. The cavity length at which power drop occurs is the mode-degenerate location. The shift in the degenerate location with absorbed pump power was due to the thermal lensing effect.

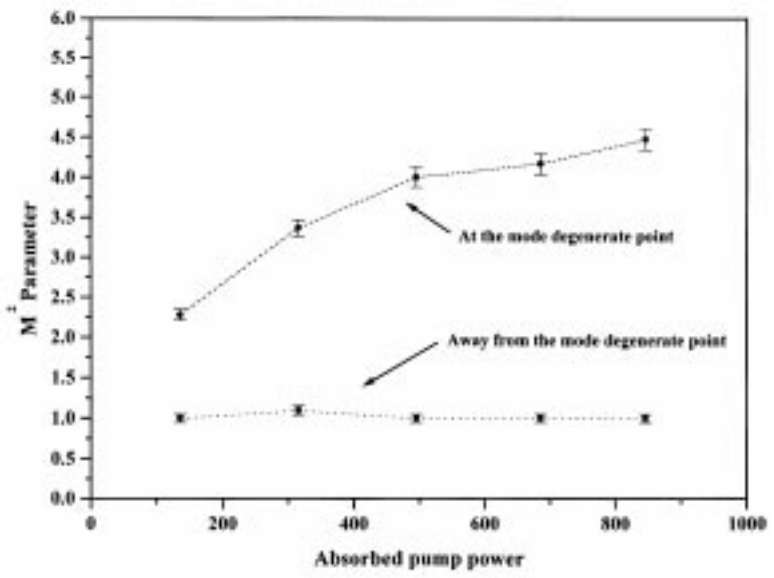

Figure 7. Beam propagation factor (M^2 parameter) vs. the absorbed pump power at and away from the mode degenerate location for 1 at.%-doped Nd : YVO_4 laser.

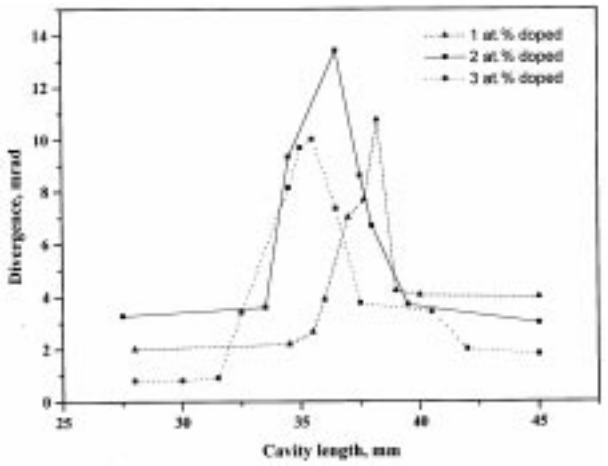

Figure 8. Variation of the output beam divergence with the cavity length for 1, 2 and 3 at.%-doped Nd : YVO_4 crystal near the fourth-order degeneracy configuration.

5. Q-switched performances

We have studied the actively Q-switched performance for Nd : YVO_4 crystal with varying doping concentration with the help of an acousto-optic modulator made of fused silica. The reason for choosing AO modulator was due to its very low insertion loss. All the measurements were done in identical cavity configuration with 5% output coupling. For

$Nd:YVO_4$ crystal the fluorescence lifetime of the upper laser level decreases with the Nd^{3+} concentration and hence the Q-switched performance is expected to deteriorate with the doping concentration. In our experimental set up with the measured intrinsic losses the pulse build up time τ_D was calculated to be of the order of the switching time, i.e., around 60 ns.

The pulse characteristics for these crystals were measured as a function of the absorbed pump power as well as the repetition rate. The pulses were recorded with the help of a biplanar photodiode. The signal from the biplanar photodiode was recorded on a digital storage oscilloscope with 100 MHz bandwidth and 400 Ms/sec sampling rate. From the oscilloscope trace we have measured the pulse width (FWHM). The pulse energy was calculated from the average power and the repetition rate as pulse energy = average power/ repetition rate. The maximum possible error was estimated as 5% in all the measurements.

In figures 9a and b we report the variation of the FWHM pulse width with the absorbed pump power and the repetition rate. For 1 and 3 at.%-doped crystals the pulse width was

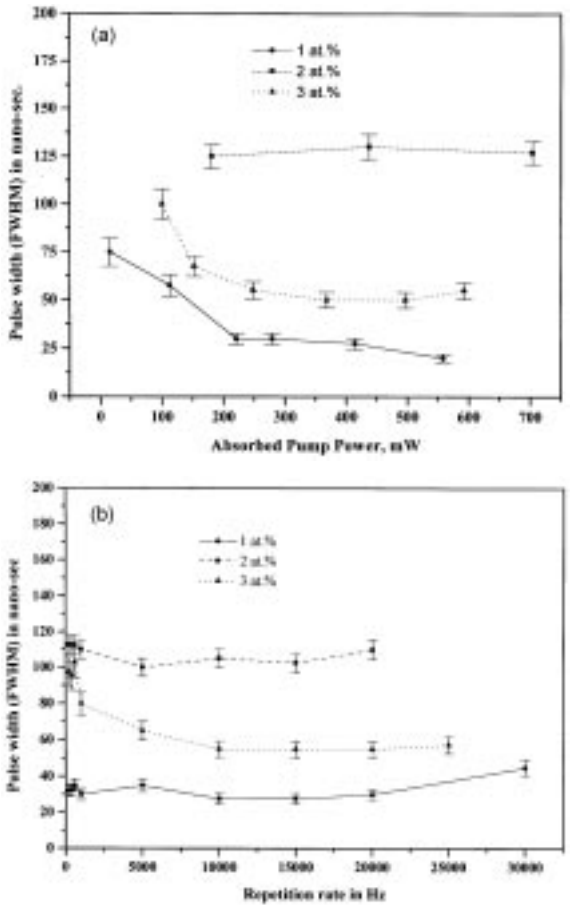

Figure 9. Variation of the pulse width (full width at half maximum) for acousto-optically Q-switched $Nd:YVO_4$ laser (**a**) with the absorbed pump power and (**b**) with the pulse repetition rate.

found to decrease with the absorbed pump power as expected, but for 2 at.%-doped crystal it remained almost constant at 125 ns. It is also to be noted that the pulses are always higher in width for 2 at.%-doped crystal compared to that of 3 at.%-doped crystal, though the energy storage capacity for 2 at.%-doped crystal is supposed to be more than that of 3 at.%-doped crystal due to its longer fluorescence life time. The reason for higher pulse width in the case of 2 at.%-doped crystal may be due to the oscillation of multilongitudinal modes. Since each longitudinal mode has different build up time, this effect may give rise to broadening of the pulses. The shortest pulse (20 ns) was obtained for 1 at.%-doped crystal at 200 Hz repetition rate at the maximum absorbed pump power.

In figure 10a and b we display the variation of the pulse energy obtained from these crystals as a function of the absorbed pump power and the repetition rate. The highest

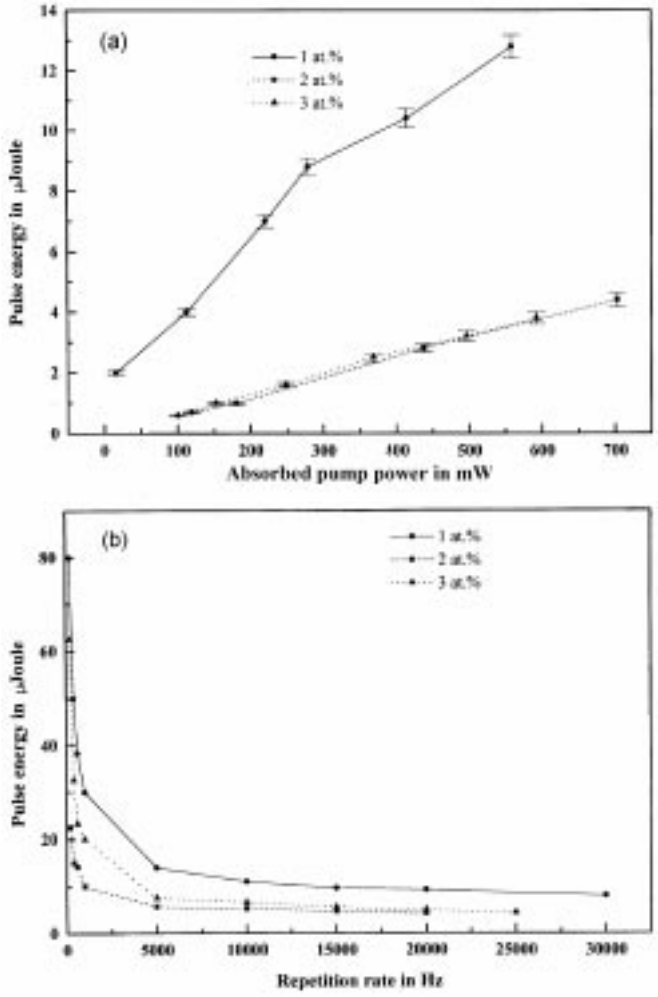

Figure 10. Variation of the pulse energy for acousto-optically Q-switched Nd : YVO_4 laser (**a**) with the absorbed pump power and (**b**) with the pulse repetition rate.

pulse energy obtained was 80 μJ for 1 at.%, 22 μJ for 2 at.% and 62 μJ for 3 at.%-doped crystal, at 100 Hz repetition rate. 1 at.%-doped crystal shows a much higher slope for pulse energy compared to the other crystals whereas 2 and 3 at.%-doped crystals show similar slope for pulse energy. With the repetition rate we also find that at low repetition rates pulses obtained from 3 at.%-doped crystal are much higher in energy than that from the 2 at%-doped crystal contrary to the expected behavior. Anyway pulses from 1 at.%-doped crystals are always higher in energy and shorter in width as expected.

6. Conclusion

In conclusion we have experimentally found the effect of Nd^{3+} concentration on CW and pulsed performance of diode pumped $Nd:YVO_4$ laser. We find that with doping concentrations the absorption efficiency increases for $Nd:YVO_4$ crystal whereas the laser performance deteriorates. The results of all these experiments can be summarized as follows: The fractional heat load for $Nd:YVO_4$ crystal increases with the doping concentration. For 1 at.%-doped crystal it is the minimum possible value, i.e., 24% whereas for 2 and 3 at.%-doped crystals it was 33 and 45% respectively. By slope efficiency measurements we found that the optimum coupling for 1 at%-doped crystal was 9% and for 2 and 3 at.%-doped crystals it was 95%. It was also found that upconversion processes are significant for higher doping level at high output coupling. Near the fourth-order degeneracy 2 at.%-doped crystal has shown maximum degradation of the beam. For Q-switched operation pulses of 80 μJ energy and widths as short as 20 ns. were obtained from 1 at.%-doped crystal. Overall we found the best performance from $Nd:YVO_4$ laser with 1 at.% doping concentration.

However, 2 at.%-doped $Nd:YVO_4$ crystals are particularly useful in making a highly compact microchip lasers which can offer single axial mode oscillation with appreciable high power. Due to its high absorption coefficient and large absorption bandwidth a tiny crystal (thickness 100–500 μm) can be used as the gain medium in order to avoid the spatial hole burning effect, whereas 1 and 3 at.%-doped crystal will not be useful for this purpose. Same way larger thickness of 1 at.%-doped crystal will be required in order to have sufficient absorption at the pump beam which may lead to multimode oscillation and though a tiny piece of 3 at.%-doped crystal can absorb the pump beam efficiently it cannot be scaled to higher power due to its large fractional thermal loading which may lead to the damage of the crystal.

References

[1] R A Fields, M Birnbaum and C L Fincher, *Appl. Phys. Lett.* **51**, 1885 (1987)
[2] Y F Chen, T M Huang, C L Wang and L J Lee, *Appl. Opt.* **37**, 5727 (1998)
[3] Y F Chen, Y P Lan and S C Wang, *Opt. Lett.* **25**, 1016 (2000)
[4] J G Sliney, K M Leung, M Birnbaum and A W Tucker, *J. Appl. Phys.* **50**, 3778 (1979)
[5] A W Tucker, M Birnbaum, C L Fincher and J W Erler, *J. Appl. Phys.* **48**, 4907 (1977)
[6] Y F Chen, *IEEE J. QE* **35**, 234 (1999)
[7] A Sennaroglu, *Opt. and Quantum Electron.* **32**, 1307 (2000)
[8] Y F Chen, T S Liao, C F Kao, T M Huang and S C Wang, *IEEE J. QE* **32**, 2010 (1996)

[9] H H Wu, C C Shu, T W Chen, M D Wei, M D Wei and W F Hsieh, *Opt. Commun.* **165**, 225 (1999)
[10] C Pfistner, R Weber, H P Weber, S Merazzi and R Gruber, *IEEE J. QE* **30**, 1605 (1994)
[11] Y Liao, R J Dwayne Muller and M R Armstrong, *Opt. Lett.* **24**, 1343 (1999)
[12] A Sennaroglu, *Appl. Opt.* **38**, 3253 (1999)
[13] Y F Chen and H J Kuo, *Opt. Lett.* **23**, 846 (1998)
[14] N Mermilloid, R Romero, I Chartier, C Garapon and R Moncorge, *IEEE J. QE* **28**, 1179 (1992)
[15] Y F Chen, Y P Lan and S C Wang, *IEEE J. QE* **36**, 615 (1996)
[16] C D Marshall, L K Smith, R J Beach, M A Emanuel, K I Schaffers, J Spidmore, S A Payne and B H T Chai, *IEEE J. QE* **32**, 650 (1996)